ROYAL SOCIETY
OF CHEMISTRY

PAPER

Check for updates

Improving the device performance of organic solar cells with immiscible solid additives†

Shuaishuai Chen,‡[a] Chengliang He,‡[a] Yaokai Li,[a] Tianyi Chen,[a] Xinxin Xia,[b] Weifei Fu,[a] Minmin Shi, [ID][a] Xinhui Lu, [ID][b] Lijian Zuo*[ac] and Hongzheng Chen [ID]*[a]

Morphology optimization is key for the high-performance of organic solar cells (OSCs). Herein, we develop a solid additive (*i.e.* uv-9) showing immiscibility with active layers for morphology control, and comprehensively study its effect on the morphology evolution and device performance of PM6:Y6 OSCs. The addition of uv-9 leads to more refined phase separation and stronger molecular packing in PM6:Y6 blend films, and improves the charge generation, exciton dissociation, charge transport and collection, which contribute to higher photocurrent and fill factor for PM6:Y6 OSCs. Consequently, the OSC device with the uv-9 solid additive exhibits an improvement in the power conversion efficiency from 16.00% to 17.18%, compared to the control device without an additive. Moreover, the generality of uv-9 as an effective solid additive has been verified by applying it to diverse OSCs. This work suggests a new class of solid additives to optimize the morphology of OSCs for high performance.

1. Introduction

Organic solar cells (OSCs) are drawing more and more attention due to their attractive advantages like light weight, low processing cost, flexibility, semi-transparency, *etc.*[1–6] With the rapid progress in material design, morphology control, device architecture design, *etc.*, the power conversion efficiency (PCE) of OSCs has been significantly improved.[7–18] At present, the PCE of OSCs based on non-fullerene acceptors (NFAs) has surged over 18%, showing great prospects for practical applications.[19–21]

The active layer film morphology is a critical factor affecting the performance of bulk heterojunction OSCs,[22] as all the pivotal processes during photon to electron conversion, *e.g.* exciton dissociation and carrier transport, can be affected by morphology.[23–29] Ideally, a nanoscale phase-separated interpenetrating network structure is favored to facilitate both exciton dissociation and charge collection.[30–32] In this context, a highly crystalline film with an optimal phase separation scale and a smooth surface can result in better carrier dynamics properties for higher device performance. The general methods used to control the morphology of the photoactive layer include solvent selection, thermal annealing (TA), solvent vapor annealing (SVA), pre-aggregation, additives, *etc.*[33–38] The key effect on the above mentioned strategy for morphology control lies in tuning the dynamics or kinetics of the donor:acceptor (D:A) phase separation during the solidification process or post-ripening. In particular, the additives are most frequently used and are proved to be critical ingredients for most high-performance OSCs.[39–42]

The pioneering work on 1,8-diiodooctane as an additive triggered the general interest in using additives to tune the morphology and improve the device performance of OSCs.[43] The previous work focused on using high-boiling point liquid as an additive such as chloronaphthalene (CN), which tends to remain in a wet active layer film after the main solvent volatilization.[44–47] Complementary to the liquid additives, recent work demonstrated the use of small molecule solids also shows a positive effect on morphology control and device performance enhancement. For example, Li *et al.* blended 1,4-difluorobenzene (DFB) into an active layer precursor solution to introduce halogen interactions in the active layer, which affect the nanoscale phase separation morphology and molecular packing.[48] Li *et al.* introduced chlorinated graphene (GCI) as a solid additive into the PM6:Y6 based device, and successfully improved the PCE of the device to 17.3%, with a high fill factor (FF) of 79%.[49] Ye *et al.* added ferrocene (Fc) into the PM6:Y6 active layer to improve the molecular crystallinity and carrier dynamics, and achieved an efficiency of 17.4%.[50] In spite of the advantages of solid additives, however, there are limited studies on it, and moreover, the fundamental understanding of the

[a] *State Key Laboratory of Silicon Materials, MOE Key Laboratory of Macromolecular Synthesis and Functionalization, Department of Polymer Science and Engineering, Zhejiang University, Hangzhou 310027, P. R. China. E-mail: zjuzlj@zju.edu.cn, hzchen@zju.edu.cn*

[b] *Department of Physics, The Chinese University of Hong Kong, Hong Kong 999077, P. R. China*

[c] *Zhejiang University-Hangzhou Global Scientific and Technological Innovation Center, Hangzhou 310014, P. R. China*

† Electronic supplementary information (ESI) available. See DOI: 10.1039/d1tc04222j

‡ These authors contributed equally to this work.

This journal is © The Royal Society of Chemistry 2022

J. Mater. Chem. C, 2022, **10**, 2749–2756 | **2749**

working mechanism of the solid additives on the morphology evolution and device performance improvement is still in need.

To enrich the pool of solid additives and provide insights into the working mechanism, here we introduce 2-hydroxy-4-methoxybenzophenone (uv-9) as a solid additive into PM6:Y6 based OSCs, and demonstrate it as an effective agent to optimize the film morphology and improve the device performance. Different from the previous study using highly miscible solids as additives, uv-9 exhibits rather high immiscibility with the active layer. After uv-9 addition, the molecular packing of the active layer is improved, and the phase separation scale becomes smaller. Correspondingly, the device prepared with uv-9 as a solid additive shows more efficient charge generation and better charge transport properties, yielding a higher short circuit current density (J_{SC}) and FF. Finally, the OSC device with uv-9 shows a much improved PCE from 16.00% to 17.18%. Furthermore, uv-9 is proved to be an effective additive that can be generally applied in a variety of OSCs.

2. Results and discussion

2.1 Photovoltaic properties

To investigate the effect of uv-9 as a solid additive on OSC device performance, we applied it to PM6:Y6 based OSCs, which consist of the indium-tinoxide(ITO)/poly(3,4-ethylene-dioxythiophene): poly(styrenesulfonate)(PEDOT:PSS)/PM6:Y6 active layer without or with different additives/poly9,9-bis6-(N,N,N-trimethylammonium) hexylfluorene-alt-co-phenylene-bromide (PFN-Br)/Ag (Fig. 1a). The chemical structures of PM6, Y6 and uv-9 are shown in Fig. 1b. The amount of the

additive uv-9 used in PM6 and Y6 is 25% (mass ratio) and an extra pre-annealing step at 100 °C for 10 min was performed for devices. The details for device fabrication can be found in the ESI.† Fig. 1c shows the current density–voltage (J–V) characteristic curves of the OSCs without or with different additives. Their photovoltaic parameters are summarized in Table 1. The device without an additive exhibits an optimal efficiency of 16.00%, with an open-circuit voltage (V_{OC}) of 0.838 V, a J_{SC} of 26.12 mA cm^{-2}, and a FF of 73.30%. The device with CN additive shows similar J_{SC} and V_{OC} values, but an increased FF of 75.37%, yielding an improved efficiency of 16.50%, while the device with uv-9 as an additive exhibits a much improved J_{SC} of 27.68 mA cm^{-2} and a FF of 76.36%, and these improvements contribute to an improved PCE of 17.18%. The statistic histograms of device parameter variations without or with different additives are summarized in Fig. 1d and e, Fig. S1 and S2 (ESI†). As shown, all devices with uv-9 exhibit a higher PCE (max: 17.18%), higher J_{SC} (max: 27.92 mA cm^{-2}), and higher FF (max: 77.08%) compared with those without any additives. These results confirm the improved device performance with uv-9 as an additive.

Considering that the improved J_{SC} is one major factor contributing to the improved device performance with uv-9 as an additive, the EQE spectra were recorded to figure out the detailed mechanisms (Fig. 1f). Without any additive, the OSC exhibits an EQE response as high as 84.1%, with the EQE edge at 932 nm, and this yields an integrated photocurrent of 25.76 mA cm^{-2}, which is consistent with the measured J_{SC} from the J–V curve (Table 1). With the CN additive, the OSC exhibits an improved EQE response to 87.8%, while its EQE spectrum
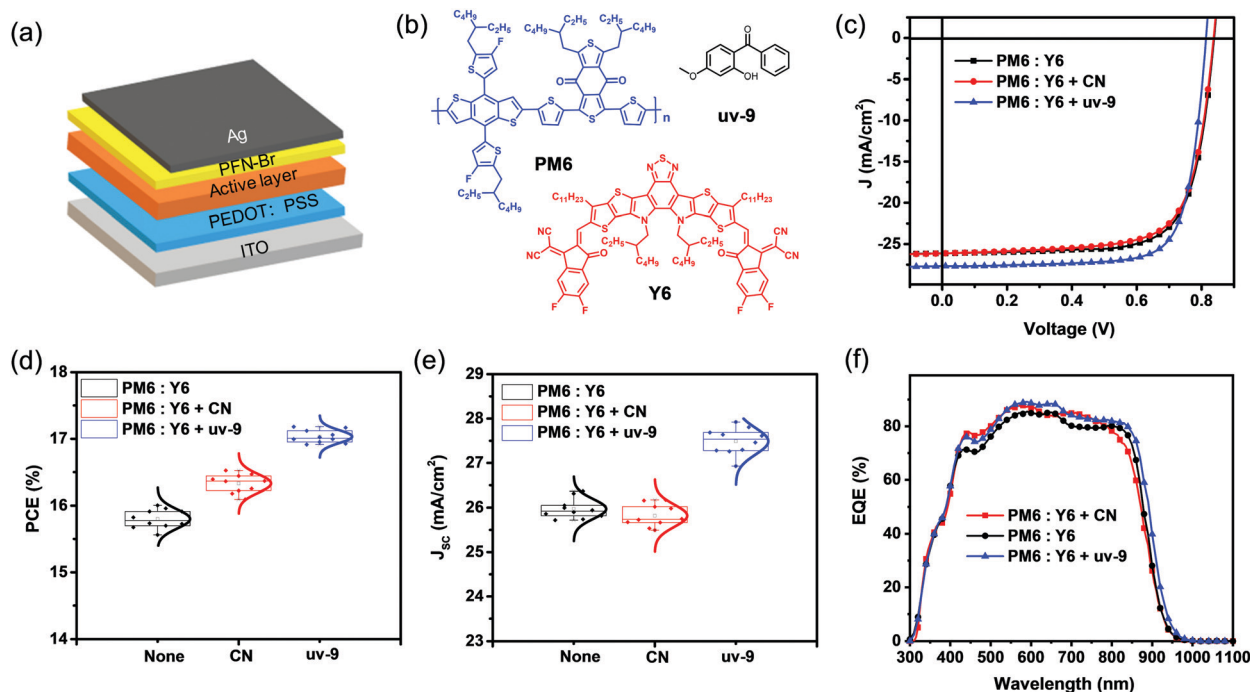

Fig. 1 (a) Schematic OSC device structure. (b) Chemical structures of PM6, Y6, and uv-9. (c) J–V characteristic curves of OSC devices with and without additives. (d) PCE statistic histogram, (e) J_{sc} statistic histogram, and (f) EQE spectra of OSCs with and without additives.

2750 | J. Mater. Chem. C, 2022, **10**, 2749–2756

This journal is © The Royal Society of Chemistry 2022

Table 1 Detailed photovoltaic parameters of OSC devices employing PM6:Y6 blends with and without additives (AD)

AD	V_{OC} (V)	J_{SC} (mA cm^{-2})	J_{cal} (mA cm^{-2})^c	FF (%)	PCE (%)
None	0.838 (0.838^a ± 0.002)	26.12 (25.97^a ± 0.21)	25.76	73.30 (72.60^a ± 0.67)	16.00^b (15.80^a ± 0.14)
CN	0.839 (0.839^a ± 0.002)	26.17 (25.91^a ± 0.24)	26.11	75.37 (75.44^a ± 0.36)	16.52^b (16.33^a ± 0.13)
uv-9	0.813 (0.814^a ± 0.001)	27.68 (27.48^a ± 0.28)	27.21	76.26 (76.21^a ± 0.63)	17.18^b (17.03^a ± 0.09)

^{a} The average value of ten devices. ^{b} The best of ten devices. ^{c} Integrated J_{SC} values from the EQE spectra.

exhibits obvious shrinkage in the absorption tail. The compromise between the improved EQE response and the shrinkage range results in the same J_{SC} compared to the device without any additive. Interestingly, the device with uv-9 as an additive exhibits both an improved EQE response (from 84.1% to 88.4%) and an extended EQE range (from 932 to 950 nm), which contributes to the much improved J_{SC} from 26.12 mA cm^{-2} to 27.68 mA cm^{-2}.

2.2 Optical properties

The absorption spectra of the active layer without or with different additives are recorded to track the origin of the broadened EQE response. In order to be consistent with the film processing conditions in the device, the annealed film was employed for the ultraviolet-visible (UV-vis) absorption measurement. The absorption spectra of the PM6:Y6 blend films with and without additives show an evident change as shown in Fig. 2a. In the Y6 absorption region, the PM6:Y6 blend film without an additive exhibits an absorption peak at 816 nm, which is slightly blue-shifted by 4 nm (812 nm) after being processed with CN, while red-shifted by 14 nm (830nm) with uv-9. To independently study the effect of additives on Y6 and PM6 aggregation, UV-vis absorption spectra are recorded for pristine Y6 and PM6 films with and without additives, as well as the pristine uv-9 film (Fig. 2b, Fig. S3 and S4 in the ESI†). A similar trend is observed compared to the PM6:Y6 blend. The absorption of Y6 is blue-shifted with the CN additive, but red-shifted with uv-9. As a result, it is confirmed that uv-9 can extend the absorption of Y6, and contribute to a higher PCE in OSCs, due to the broadened absorption. Furthermore, the red-shifted absorption indicates that the molecular packing

becomes stronger, which benefits the carrier dynamics processes, e.g. charge transport.

2.3 Charge transport and collection

A higher FF and EQE response with uv-9 addition indicate that the carrier dynamics within OSCs is improved, including the exciton dissociation, charge transport, charge collection and recombination. First, the charge transport characteristics of the device in the vertical direction were studied by the Space Charge Limited Current (SCLC) method. As shown in Fig. 3a and b and Table S1 (ESI†), the hole mobility of the film without an additive is 4.12×10^{-4} cm^{-2} V^{-1} s^{-1}, while the devices with CN and uv-9 as additives show increased hole mobilities of 4.52×10^{-4} cm^{-2} V^{-1} s^{-1} and 6.14×10^{-4} cm^{-2} V^{-1} s^{-1}, respectively. Furthermore, devices using uv-9 as a solid additive show increased electron mobilities from 6.25×10^{-4} cm^{-2} V^{-1} s^{-1} to 9.12×10^{-4} cm^{-2} V^{-1} s^{-1}, while the electron mobility of the device with CN is only 5.17×10^{-4} cm^{-2} V^{-1} s^{-1}. Both the electron and hole mobilities of the devices with uv-9 as a solid additive increase, which contributes to the high FF.

In order to study the influence of the uv-9 additive on the process of charge extraction, we measured the effective voltage (V_{eff}) dependent photocurrent density (J_{ph}, $J_{ph} = J_L - J_{dark}$, where J_L is the current density measured under AM1.5G illumination, J_{dark} is measured under dark conditions; $V_{eff} = V_0 - V$, where V_0 is the voltage at $J_{ph} = 0$) as shown in Fig. 3c and d. The OSC device with uv-9 exhibits a significantly larger J_{ph} value at a small V_{eff} value compared to those without or with the CN additive, suggesting the improved charge collection. By assuming that all excitons can be separated into free carriers and collected by the electrode to form a saturation current
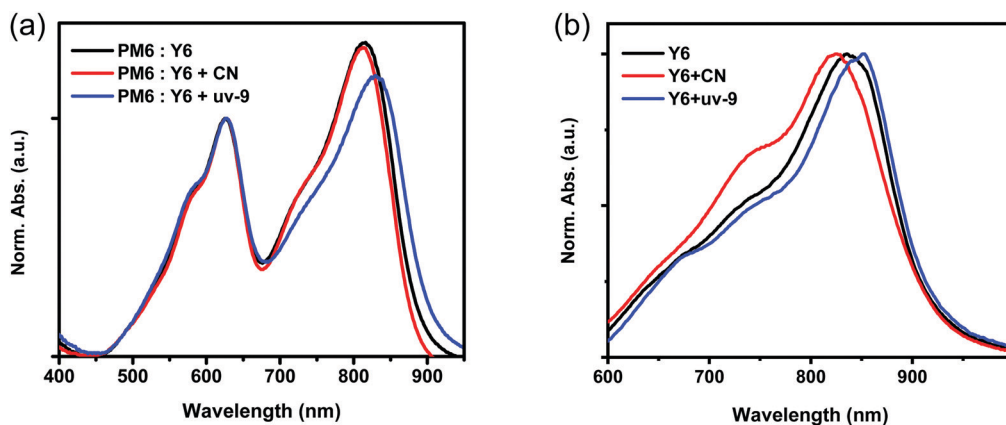

Fig. 2 UV-Vis absorption spectra of (a) PM6:Y6 blend and (b) Y6 films with and without additives.

Fig. 3 (a) $J^{0.5}$–V curves of the electron-only devices. (b) $J^{0.5}$–V curves of the hole-only devices. (c) Photocurrent density (J_{ph}) plotted against effective bias (V_{eff}) for devices without or with different additives. (d) Dark J–V curves, (e) J_{SC} and (f) V_{OC} *versus* light intensity of devices with and without additives.

(J_{sat}, defined as the photocurrent at a bias of 2 V), the charge collection probability P_{coll} can be calculated through the relationship $P_{coll} = J_{ph}/J_{sat}$, and the charge collection probability of the device with uv-9 as a solid additive is as high as 97.1% at 0 V, while the charge collection probabilities of the devices with and without the CN additive is 94.8% and 95.4%, respectively. These results confirm that the addition of uv-9 can promote charge extraction, thereby improving the FF and J_{SC} of OSC devices.

2.4 Charge recombination

The dependence of J_{SC} and V_{OC} on the light intensity (P_{light}) was measured to explore charge recombination behaviors in the above OSC devices. Generally, the relationship between J_{SC} and P_{light} can be described as $J_{SC} \propto (P_{light})^S$. As shown in Fig. 3e, the S value of the device with uv-9 is 0.97, which is slightly higher than those of the devices with CN as the additive and without an additive (0.96). The S closer to 1 suggests the lower bimolecular recombination in the device.[51] As a result, this proves that the bimolecular recombination under short circuit conditions can be inhibited, in other words, more efficient charge extraction can be achieved with the addition of uv-9. By calculating the slope in V_{OC}–ln P_{light}, the main recombination mechanism under open circuit conditions in the device can be inferred. As shown in Fig. 3f, the slope of the V_{OC}–P_{light} curve of the devices without and with CN and uv-9 is 1.12 k_BT/q, 1.14 k_BT/q and 1.18 k_BT/q, respectively, indicating that their charge recombination mechanism is mainly *via* a bimolecular mechanism in all cases.

2.5 Morphology characterization

Atomic force microscopy (AFM) and grazing incidence small-angle X-ray scattering (GISAXS) methods were used to study the film morphology of the active layer. As shown in Fig. 4a–c, the root mean square (RMS) values of the PM6:Y6 film, PM6:Y6 film with CN and PM6:Y6 film with uv-9 are 0.656 nm, 0.708 nm, and 0.713 nm, respectively, showing an increasing tendency. From the GISAXS results, the phase-separation domain (pure acceptor phase) of the three films shows a decreasing trend, which is 29 nm, 27 nm, and 25 nm, as displayed in Fig. 4d–f (the scattering intensity is fitted by the Born Approximation model in Fig. 4g). Compared to those without an additive or with CN, the film with the uv-9 additive shows a slightly reduced phase region scale, which is beneficial for exciton separation or charge generation. Furthermore, we find that the 25 nm domain size causes little negative effect on charge transport or charge collection. As a result, the reduced phase separation domain size (25 nm) represents a better balance between charge separation and charge transport. These results indicate that the addition of uv-9 can optimize the morphology by refining the phase separation and enhancing the molecular packing. The enhanced molecular packing of Y6 contributes to the red-shifted UV-vis absorption profiles or the reduced E_g, which further results in decreased V_{OC} values (Table S2, ESI†).

2.6 Working mechanism of the uv-9 additive

Fourier transform infrared (FT-IR) measurements were performed to check the existence of uv-9 in the active layer/precursors during different stages. In the PM6:Y6 blend film
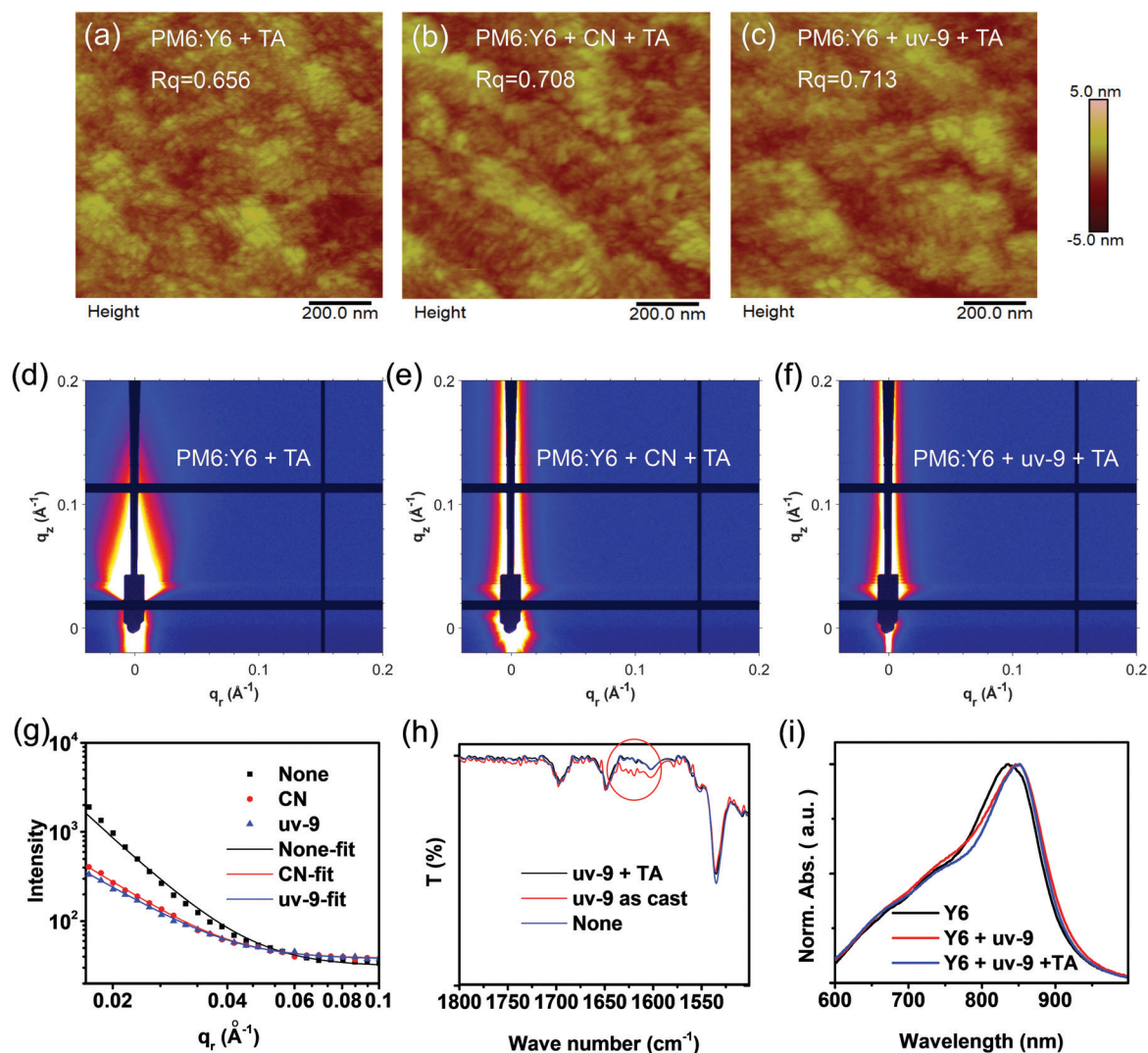
Fig. 4 AFM height images of PM6:Y6 blend films without additive (a) and with additives of CN (b) and uv-9 (c), in a scan size of $1 \times 1\ \mu m^2$. 2D GISAXS images of PM6:Y6 blend films without additive (d) and with additives of CN (e) and uv-9 (f). (g) 1D in-plane intensity profiles and fitting curves of blend films with and without additive. (h) FT-IR spectra of PM6:Y6 blend films with and without uv-9 additive. (i) UV-vis absorption spectra of Y6 and Y6:uv-9 blend films before and after thermal annealing.

with the addition of uv-9, the stretching vibration peak of the benzophenone carbonyl group increases significantly (at 1630–1650 cm^{-1}), suggesting the existence of uv-9 in the as-prepared active layers (Fig. 4h). However, after annealing, this feature peak disappears, and the spectrum overlaps with that without any additive, suggesting that there is no residue of uv-9 additives in the active layer after thermal annealing. The disappearance of uv-9 was also observed in the Y6 film with the addition of uv-9 after annealing (Fig. S5 in the ESI†). The photostability of uv-9 based OSC devices was studied. Compared to the control devices (without uv-9), the devices with uv-9 show similar PCE decline tendency after preserving in an inert atmosphere under simulated solar illumination (Fig. S6, ESI†). However, this is quite reasonable considering that uv-9 disappears after thermal annealing as revealed by FTIR results (Fig. 4h). Fig. 4i and Fig. S7 (ESI†) show the absorption profiles

of the Y6 film processed with uv-9 before and after annealing at different times. It is interesting to observe that the as-prepared Y6:uv-9 film exhibits a red-shift compared to the pure Y6 film, and the absorption of the Y6:uv-9 blend exhibits little difference compared with that before annealing. These results suggest that the phase separation and molecular packing have already formed in the as-prepared active layer films prior to the removal of uv-9 by annealing. Fig. S8 (ESI†) shows the UV-vis absorption spectra of Y6:uv-9 blend films with different mass ratios. We find that increasing the content of uv-9 (uv9 : Y6 = 3 : 7 or 5 : 5) does not lead to any red-shifts in the absorption spectra of Y6 films. This result also indicates that uv-9 is immiscible with Y6.

Following the above observation, the miscibility of uv-9 with PM6 and Y6 was studied by measuring the surface energy (γ) of the material. Fig. S9 (ESI†) and Table 2 show the contact angles

This journal is © The Royal Society of Chemistry 2022

J. Mater. Chem. C, 2022, **10**, 2749–2756 | **2753**

Table 2 Contact angle and Flory–Huggins interaction parameters of the films

Surface	θ water [°]	θ diiodomethane [°]	γ [mN m^{-1}]	χ^{D-A}
PM6	103.50	55.94	31.88	—
Y6	93.11	43.58	38.01	0.27
Y6 + uv-9	94.98	43.22	38.23	0.29
uv-9	32.07	25.87	64.82	—

of PM6, Y6 and uv-9 with water and diiodomethane, respectively. The calculated surface energy of PM6 (γ = 31.88 mN m^{-1}) is lower than that of Y6 (γ = 38.01 mN m^{-1}), much lower than the surface energy of uv-9 (γ = 64.82 mN m^{-1}). The Flory–Huggins interaction parameter $\chi^{1,2}$ was used to estimate the miscibility between PM6/Y6 and uv-9, according to the previous report.[52] The $\chi^{1,2}$ parameter value of Y6 and uv-9 is 3.557, and that of PM6 and uv-9 is 5.784. Considering that the measured $\chi^{1,2}$ value of PM6 and Y6 is 0.27, it is clear that uv-9 is an immiscible component for the active layer (Table S3, ESI†). However, we observe that uv-9 and chloroform are quite miscible, as homogeneous mixing is observed even when a huge amount of uv-9 is dissolved in chloroform (Fig. S10, ESI†), in spite of the surface tension difference between chloroform and uv-9.

Based on the above information, the working mechanism of uv-9 is proposed as follows. First, the addition of uv-9 changes the miscibility among the donor, acceptors and solvents, and thermodynamically affects the phase-separation and molecular packing of the active layer. In addition, hydrogen bonds may be formed between uv-9 (–OH) and PM6/Y6 (–F), and further affect the molecular packing of Y6, *via* influencing the molecular aggregation in solution or during the film solidification process. Furthermore, uv-9 has a high melting point at 62 °C, which is above room temperature, and it has been observed that the chloroform:uv-9 blend with a weight ratio of 1:9 appears as a solid (melting point above room temperature) (Fig. S10 in the ESI†). Considering the high miscibility between chloroform and uv-9, it is reasonable that the residual chloroform tends to mix with uv-9 to form a solid phase, rather than affecting the afterward phase-segregation process. As a result, uv-9 addition is proposed to affect the phase-separation

kinetics *via* deactivating the effect of the residual solvent (chloroform) for morphology evolution.

2.7 Generality of uv-9 as an additive

Finally, we investigated the applicability of uv-9 as a solid additive in diverse systems utilizing PM6 as the donor, and PC$_{71}$BM, IT4F and ITIC as acceptors. The chemical structures of PC$_{71}$BM, IT4F and ITIC are shown in Fig. S11 (ESI†). uv-9 with 25% content (by weight%) was used as an additive in the active layers. The J–V characteristic curves of these OSCs without and with uv-9 addition are shown in Fig. 5, and their photovoltaic parameters are summarized in Table S4 (ESI†). Compared with devices without additives, the devices using uv-9 as solid additives have higher J_{SC} and FF values, and also higher PCE values for all of the three systems. The results validate that uv-9 is an effective additive that can be generally used in other systems to control the morphology and improve the performance of organic solar cells.

3. Conclusions

In summary, we have successfully demonstrated uv-9 as an effective solid additive to tune the morphology and improve the device performance of binary organic solar cells based on PM6:Y6. The addition of uv-9 refines the phase separation domain size and enhances the molecular packing. As a result, charge separation and collection are improved, and the absorption region is extended, which contribute to enhanced short circuit current densities, fill-factors and device performances from 16.00% to 17.18%. Further analysis suggests that the morphology evolution of uv-9 might be related to its immiscibility with the active layer but high miscibility with the main solvent, which affects both the phase separation dynamics and kinetics. Moreover, the effectiveness of uv-9 has been confirmed in diverse organic solar cells, demonstrating its generality to tune the morphology and improve the device performance of organic solar cells.

Conflicts of interest

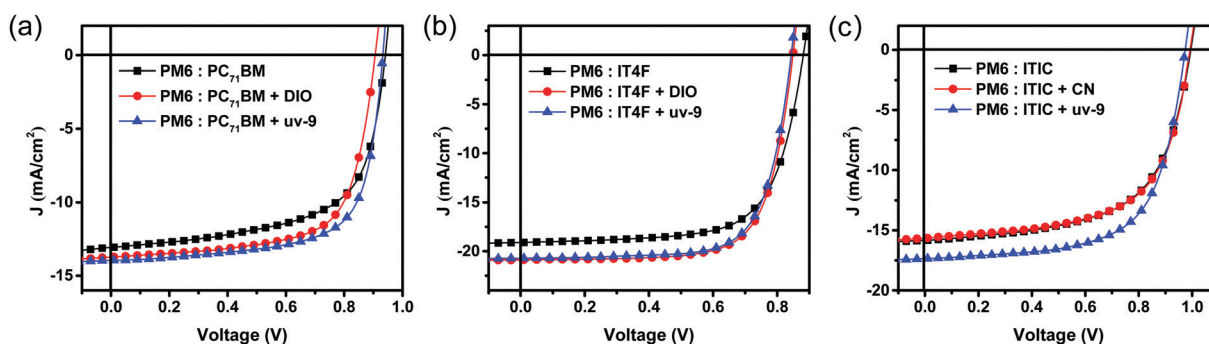The authors declare that there is no conflict of interest.

Fig. 5 J–V characteristics of (a) PM6:PC$_{71}$BM, (b) PM6:IT4F, and (c) PM6:ITIC based OSC devices with and without additives.

2754 | *J. Mater. Chem. C*, 2022, **10**, 2749–2756

This journal is © The Royal Society of Chemistry 2022

Acknowledgements

References

1 S. Chen, G. Zhang, J. Liu, H. Yao, J. Zhang, T. Ma, Z. Li and H. Yan, *Adv. Mater.*, 2017, **29**, 1604231.

2 Y. Li, J. D. Lin, X. Che, Y. Qu, F. Liu, L. S. Liao and S. R. Forrest, *J. Am. Chem. Soc.*, 2017, **139**, 17114–17119.

3 J. Zhao, Y. Li, G. Yang, K. Jiang, H. Lin, H. Ade, W. Ma and H. Yan, *Nat. Energy*, 2016, **1**, 15027.

4 Y. Li, C. He, L. Zuo, F. Zhao, L. Zhan, X. Li, R. Xia, H. Yip, C. Li, X. Liu and H. Chen, *Adv. Energy Mater.*, 2021, **11**, 2003408.

5 F. Zhao, L. Zuo, Y. Li, L. Zhan, S. Li, X. Li, R. Xia, H. Yip and H. Chen, *Sol. RRL*, 2021, 2100339.

6 Y. Su, S. Lan and K. Wei, *Mater. Today*, 2012, **15**, 554–562.

7 S. Geng, W. Yang, J. Gao, S. Li, M. Shi, T. Lau, X. Lu, C. Li and H. Chen, *Chin. J. Polym. Sci.*, 2019, **37**, 1005–1014.

8 H. Bin, L. Gao, Z. G. Zhang, Y. Yang, Y. Zhang, C. Zhang, S. Chen, L. Xue, C. Yang, M. Xiao and Y. Li, *Nat. Commun.*, 2016, **7**, 13651.

9 R. Qin, D. Wang, G. Zhou, Z. Yu, S. Li, Y. Li, Z. Liu, H. Zhu, M. Shi, X. Lu, C. Li and H. Chen, *J. Mater. Chem. A*, 2019, **7**, 27632–27639.

10 S. Li, C. Li, M. Shi and H. Chen, *ACS Energy Lett.*, 2020, **5**, 1554–1567.

11 K. Cnops, G. Zango, J. Genoe, P. Heremans, M. V. Martinez-Diaz, T. Torres and D. Cheyns, *J. Am. Chem. Soc.*, 2015, **137**, 8991–8997.

12 J. Yuan, Y. Zhang, L. Zhou, G. Zhang, H. Yip, T. Lau, X. Lu, C. Zhu, H. Peng, P. A. Johnson, M. Leclerc, Y. Cao, J. Ulanski, Y. Li and Y. Zou, *Joule*, 2019, **3**, 1140–1151.

13 L. Zhan, S. Li, X. Xia, Y. Li, X. Lu, L. Zuo, M. Shi and H. Chen, *Adv. Mater.*, 2021, **33**, 2007231.

14 Y. Lin, J. Wang, Z. Zhang, H. Bai, Y. Li, D. Zhu and X. Zhan, *Adv. Mater.*, 2015, **27**, 1170–1174.

15 J. Liu, S. Chen, D. Qian, B. Gautam, G. Yang, J. Zhao, J. Bergqvist, F. Zhang, W. Ma, H. Ade, O. Inganäs, K. Gundogdu, F. Gao and H. Yan, *Nat. Energy*, 2016, **1**, 16089.

16 A. Karki, J. Vollbrecht, A. J. Gillett, S. S. Xiao, Y. Yang, Z. Peng, N. Schopp, A. L. Dixon, S. Yoon, M. Schrock, H. Ade, G. N. M. Reddy, R. H. Friend and T. Nguyen, *Energy Environ. Sci.*, 2020, **13**, 3679–3692.

17 P. Cheng, G. Li, X. Zhan and Y. Yang, *Nat. Photonics*, 2018, **12**, 131–142.

18 H. Cheng, C. Juan, A. Mohapatra, C. Chen, Y. Lin, B. Chang, P. Cheng, H. Wang, C. W. Chu, Y. Yang and K. Wei, *Nano Lett.*, 2021, **21**, 2207–2215.

19 Y. Cui, H. Yao, J. Zhang, K. Xian, T. Zhang, L. Hong, Y. Wang, Y. Xu, K. Ma, C. An, C. He, Z. Wei, F. Gao and J. Hou, *Adv. Mater.*, 2020, **32**, 1908205.

20 K. Jin, Z. Xiao and L. Ding, *J. Semicond.*, 2021, **42**, 10502.

21 C. Li, J. Zhou, J. Song, J. Xu, H. Zhang, X. Zhang, J. Guo, L. Zhu, D. Wei, G. Han, J. Min, Y. Zhang, Z. Xie, Y. Yi, H. Yan, F. Gao, F. Liu and Y. Sun, *Nat. Energy*, 2021, **6**, 605–613.

22 F. Zhao, C. Wang and X. Zhan, *Adv. Energy Mater.*, 2018, **8**, 1703147.

23 Y. Huang, E. J. Kramer, A. J. Heeger and G. C. Bazan, *Chem. Rev.*, 2014, **114**, 7006–7043.

24 L. Zhu, M. Zhang, G. Zhou, T. Hao, J. Xu, J. Wang, C. Qiu, N. Prine, J. Ali, W. Feng, X. Gu, Z. Ma, Z. Tang, H. Zhu, L. Ying, Y. Zhang and F. Liu, *Adv. Energy Mater.*, 2020, **10**, 1904234.

25 C. He, Y. Li, S. Li, Z. Yu, Y. Li, X. Lu, M. Shi, C. Li and H. Chen, *ACS Appl. Mater. Interfaces*, 2020, **12**, 16700–16706.

26 C. He, Y. Li, Y. Liu, Y. Li, G. Zhou, S. Li, H. Zhu, X. Lu, F. Zhang, C. Li and H. Chen, *J. Mater. Chem. A*, 2020, **8**, 18154–18161.

27 S. Li, L. Zhan, Y. Jin, G. Zhou, T. K. Lau, R. Qin, M. Shi, C. Z. Li, H. Zhu, X. Lu, F. Zhang and H. Chen, *Adv. Mater.*, 2020, **32**, 2001160.

28 L. Zhan, S. Li, T. Lau, Y. Cui, X. Lu, M. Shi, C. Li, H. Li, J. Hou and H. Chen, *Energy Environ. Sci.*, 2020, **13**, 635–645.

29 S. Li, L. Zhan, N. Yao, X. Xia, Z. Chen, W. Yang, C. He, L. Zuo, M. Shi, H. Zhu, X. Lu, F. Zhang and H. Chen, *Nat. Commun.*, 2021, **12**, 4627.

30 T. L. Benanti and D. Venkataraman, *Photosynth. Res.*, 2006, **87**, 73–81.

31 T. Liu, L. Huo, S. Chandrabose, K. Chen, G. Han, F. Qi, X. Meng, D. Xie, W. Ma, Y. Yi, J. M. Hodgkiss, F. Liu, J. Wang, C. Yang and Y. Sun, *Adv. Mater.*, 2018, **30**, 1707353.

32 R. Singh, J. Lee, M. Kim, P. E. Keivanidis and K. Cho, *J. Mater. Chem. A*, 2017, **5**, 210–220.

33 Z. Fu, X. Liu, Y. Wang, S. Du, J. Tong, J. Li, R. Zhang, C. Yang and Y. Xia, *Sol. Energy*, 2021, **218**, 375–382.

34 K. Gao, S. B. Jo, X. Shi, L. Nian, M. Zhang, Y. Kan, F. Lin, B. Kan, B. Xu, Q. Rong, L. Shui, F. Liu, X. Peng, G. Zhou, Y. Cao and A. K. Y. Jen, *Adv. Mater.*, 2019, **31**, 1807842.

35 J. Wang, K. Liu, J. Yan, Z. Wu, F. Liu, F. Xiao, Z. Chang, H. Wu, Y. Cao and T. P. Russell, *J. Am. Chem. Soc.*, 2016, **138**, 7687–7697.

36 H. Gao, Y. Sun, Y. Cai, X. Wan, L. Meng, X. Ke, S. Li, Y. Zhang, R. Xia, N. Zheng, Z. Xie, C. Li, M. Zhang, H. Yip, Y. Cao and Y. Chen, *Adv. Energy Mater.*, 2019, **9**, 1901024.

37 X. Song, N. Gasparini, L. Ye, H. Yao, J. Hou, H. Ade and D. Baran, *ACS Energy Lett.*, 2018, **3**, 669–676.

38 D. Khatiwada, S. Venkatesan, Q. Chen, J. Chen, N. Adhikari, A. Dubey, A. F. Mitul, L. Mohammed and Q. Qiao, *J. Mater. Chem. A*, 2015, **3**, 15307–15313.

39 S. J. Lou, J. M. Szarko, T. Xu, L. Yu, T. J. Marks and L. X. Chen, *J. Am. Chem. Soc.*, 2017, **139**, 8777.

40 W. Yang, Z. Luo, R. Sun, J. Guo, T. Wang, Y. Wu, W. Wang, J. Guo, Q. Wu, M. Shi, H. Li, C. Yang and J. Min, *Nat. Commun.*, 2020, **11**, 1218.

This journal is © The Royal Society of Chemistry 2022

J. Mater. Chem. C, 2022, **10**, 2749–2756 | **2755**

41 D. Hu, Q. Yang, H. Chen, F. Wobben, V. M. Le Corre, R. Singh, T. Liu, R. Ma, H. Tang, L. J. A. Koster, T. Duan, H. Yan, Z. Kan, Z. Xiao and S. Lu, *Energy Environ. Sci.*, 2020, **13**, 2134–2141.

42 Z. Li, W. Zhong, L. Ying, N. Li, F. Liu, F. Huang and Y. Cao, *Chin. J. Polym. Sci.*, 2020, **38**, 323–331.

43 J. K. Lee, W. L. Ma, C. J. Brabec, J. Yuen, J. S. Moon, J. Y. Kim, K. Lee, G. C. Bazan and A. J. Heeger, *J. Am. Chem. Soc.*, 2008, **130**, 3619–3623.

44 H. Liao, C. Ho, C. Chang, M. Jao, S. B. Darling and W. Su, *Mater. Today*, 2013, **16**, 326–336.

45 C. Mcdowell, M. Abdelsamie, M. F. Toney and G. C. Bazan, *Adv. Mater.*, 2018, **30**, 1707114.

46 M. Su, C. Kuo, M. Yuan, U. Jeng, C. Su and K. Wei, *Adv. Mater.*, 2011, **23**, 3315–3319.

47 C. Liu, Y. Su, J. Jiang, H. Chen, S. Lin, C. Su, U. Jeng and K. Wei, *J. Mater. Chem. A*, 2014, **2**, 20760–20769.

48 S. Li, Q. Ma, S. Chen, L. Meng, J. Zhang, Z. Zhang, C. Yang and Y. Li, *J. Mater. Chem. C*, 2020, **8**, 15296–15302.

49 L. Liu, Y. Kan, K. Gao, J. Wang, M. Zhao, H. Chen, C. Zhao, T. Jiu, A. K. Y. Jen and Y. Li, *Adv. Mater.*, 2020, **32**, 1907604.

50 L. Ye, Y. Cai, C. Li, L. Zhu, J. Xu, K. Weng, K. Zhang, M. Huang, M. Zeng, T. Li, E. Zhou, S. Tan, X. Hao, Y. Yi, F. Liu, Z. Wang, X. Zhan and Y. Sun, *Energy Environ. Sci.*, 2020, **13**, 5117–5125.

51 A. K. K. Kyaw, D. H. Wang, V. Gupta, W. L. Leong, L. Ke, G. C. Bazan and A. J. Heeger, *ACS Nano*, 2013, **7**, 4569–4577.

52 S. Nilsson, A. Bernasik, A. Budkowski and E. Moons, *Macromolecules*, 2007, **40**, 8291–8301.